

Article

Upconversion Nanoparticles Encapsulated with Amorphous Silica and Their Emission Quenching by FRET: A Nanosensor Excited by NIR for Mercury Detection

Wei Wu^{1,2}, Wei Wei^{1,2}, Dingli Xu³, Yunpeng Liu⁴, Jin Li^{5,*}, Kaifeng Gan^{5,*} and Liang Liu⁶

¹ Hwa Mei Hospital, University of Chinese Academy of Sciences, Ningbo 315010, China; fiennes.wu@foxmail.com (W.W.); weiwei_nb@163.com (W.W.)

² Ningbo Institute of Life and Health, University of Chinese Academy of Sciences, Ningbo 315010, China

³ The Affiliated Hospital of Medical School of Ningbo University, Ningbo 315000, China; xudingliwo@126.com

⁴ Faculty of Electronics & Computer, Zhejiang Wanli University, Ningbo 315000, China; liuyppjoy@163.com

⁵ Li Huili Hospital Affiliated to Ningbo University, Ningbo 315211, China

⁶ School of Materials Science & Engineering, Jiangsu University, Zhenjiang 212013, China; reserch419@outlook.com

* Correspondence: lijin@nbu.edu.cn (J.L.); gankaifeng@nbu.edu.cn (K.G.)

Abstract: Near-infrared (NIR) region has been considered as a diagnostic window since it avoids sample autofluorescence and light scattering. Upconversion nanoparticles (UCNPs) convert NIR light into high energy excitation light, making them a suitable excitation source for nanoprobes with deep penetration depth and high signal-to-noise ratio. The current work reported a rhodamine-derived probe for the detection of Hg(II). Corresponding absorption and emission responses for Hg(II) and detailed recognizing mechanism were discussed. An absorption titration experiment was performed. It was found that Hg(II) directly bonded with probe with chemical stoichiometry of 1:1, its association constant was calculated as $2.59 \times 10^5 \text{ M}^{-1}$. Such a high value indicated a direct coordination affinity between Hg(II) and this rhodamine-derived probe. Most metal cations exerted no increasing effect on the probe emission or absorption, exhibiting good sensing selectivity of probe towards Hg(II). Upconversion nanoparticles (UCNPs) were firstly encapsulated with silica (SiO₂) and then bonded with the probe via a covalent bond. Given a near-infrared (NIR) laser excitation with wavelength of 980 nm, this probe, (E)-2-((3',6'-bis(diethylamino)-2',7'-dimethyl-3-oxospiro[isindoline-1,9'-xanthen]-2-yl)imino)acetaldehyde (denoted as RHO), captured the energy of UCNPs via a FRET (fluorescence resonance energy transfer) path, resulting in the emission quenching of UCNPs. This composite system showed linear sensing behavior towards Hg(II) with high selectivity, which was similar to the case of pure probe. No probe emission, however, was observed from the composite system, which was different from the case of most literature reports. The self-quenching between probe molecules was claimed responsible for the probe emission, which was confirmed by experiment result and analysis. To the best of our knowledge, this is the first demonstration of covalently integrating SiO₂-coated UCNPs with a rhodamine-derived probe for Hg(II) sensing.

Keywords: UCNPs; IR laser excitation; SiO₂ encapsulation; mercury cation



Citation: Wu, W.; Wei, W.; Xu, D.; Liu, Y.; Li, J.; Gan, K.; Liu, L. Upconversion Nanoparticles Encapsulated with Amorphous Silica and Their Emission Quenching by FRET: A Nanosensor Excited by NIR for Mercury Detection. *Crystals* **2021**, *11*, 104. <https://doi.org/10.3390/cryst11020104>

Received: 23 December 2020

Accepted: 18 January 2021

Published: 25 January 2021

Publisher's Note: MDPI stays neutral with regard to jurisdictional claims in published maps and institutional affiliations.



Copyright: © 2021 by the authors. Licensee MDPI, Basel, Switzerland. This article is an open access article distributed under the terms and conditions of the Creative Commons Attribution (CC BY) license (<https://creativecommons.org/licenses/by/4.0/>).

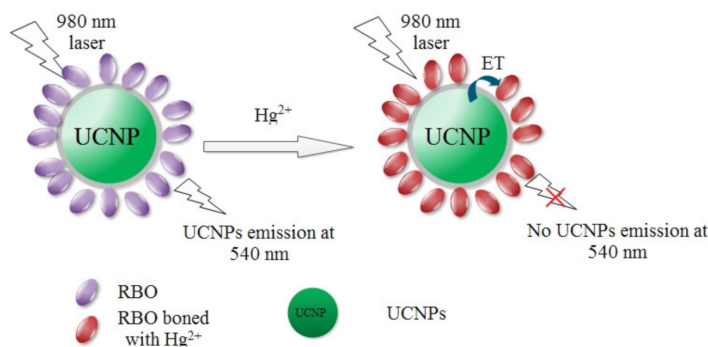
1. Introduction

Mercury and its compounds are widely distributed in natural environment and industrial manufactory. They have been classified as the most toxic matters and thus are considered as a human health threat [1]. Unfortunately, mercury and its compounds are not degradable and consequently accumulated via food chain, bringing more harm to the top terminal of the food chain, which means human beings. Human brains and nervous systems are most sensitive to mercury and its compounds [1,2]. In this case, the identification and recognition of Hg²⁺ ions and water-soluble compounds have been

listed as a critical task in environmental protection and medical treatment. As a representative analyte, Hg^{2+} is usually used to develop Hg-sensing systems. There have been Hg^{2+} -sensing systems based on pure organic probes and nanomaterials [3–6], which are, however, usually excited by high energy light within UV region. An obvious problem is the autofluorescence and thus low signal-to-noise ratio which compromises sensing performance and photo-oxidizes sensing probes. A secondary energy transfer mechanism has been proposed to solve this issue, using near-infrared (NIR) laser as excitation energy [7,8]. As a consequence, the development for sensing probes excited by NIR laser have harvested much research attention.

In most NIR-excited sensing systems, a secondary energy transfer mechanism is applied, using upconversion nanoparticles (UCNPs) as the secondary excitation source. UCNPs convert the low-energy NIR emission into high energy and then excite sensing probes, which has attracted research interests in the fields of analytical sensing and bio-imaging [9–11]. Many literatures have concluded the virtues of using UCNPs as the secondary excitation source, including long-range Stokes shift, good biocompatibility, low background luminescence noise and deep penetration depth in bio-samples [12–15]. Some sensing systems have been successfully developed for the recognition of DNA, avidin, cations and anions [16–18]. A problem facing these UCNPs is their hydrophobic surface which is highly incompatible with Hg^{2+} ions in aqueous media, leading to phase separation and thus poor sensing performance. Modifying the hydrophobic surface of UCNPs is then proposed to solve this problem. Dionne and coworkers have reported the Forster resonant energy transfer in a core-shell-shell structure with bright upconversion emission [19]. Lee and coworkers developed a NIR-to-NIR LRET system for homogeneous competitive immunoassay based on UCNPs [20]. Liu and coworkers reported a review article about the strategy for constructing upconversion luminescence nanoprobe to improve signal contrast [21]. In the meanwhile, the modification of UCNPs inevitably increases their size and compromises their fluent energy transfer to energy acceptors such as sensing probes.

In the present work, we encapsulate hydrophobic UCNPs with amorphous silica (SiO_2) which is highly hydrophilic. Then a rhodamine-derived probe (E)-2-((3',6'-bis(diethylamino)-2',7'-dimethyl-3-oxospiro[isoinoline-1,9'-xanthen]-2-yl)imino)acetaldehyde (denoted as RBO) is covalently immobilized onto this SiO_2 layer, acting as the energy acceptor for UCNPs. Given the excitation of NIR laser, this composite structure is supposed to show a selective and sensitive recognition for Hg^{2+} ions with low autofluorescence noise. Scheme 1 details the design route for this composite structure which is mentioned as UCNPs@ SiO_2 -RBO. Bright green emission light is observed by naked eyes from UCNPs@ SiO_2 -RBO nanoparticles under the excitation of NIR laser of 980 nm. With increasing Hg^{2+} concentrations, this upconversion emission is quenched obviously, showing emission quenching signal. On the other hand, there is no obvious increasing RBO emission during this procedure. A primary analysis suggests that RBO emission energy is consumed via a non-radiative path via the self-absorption of ground state RBH molecules.



Scheme 1. The design route for upconversion nanoparticles (UCNPs)@ SiO_2 -RBO and its working strategy.

2. Experimental Section

2.1. Reagents

The starting chemical reagents were purchased and used as they were with no purifications. RE oxides, including Y_2O_3 , Yb_2O_3 and Er_2O_3 , were supplied by Yingshui Chemical Reagent Company. Corresponding RE chlorides, including YCl_3 , $YbCl_3$ and $ErCl_3$, were synthesized by soaking RE oxides in concentrated HCl and then vaporizing excess solvent water. Bulk crystals were obtained by vacuum evaporation at 30 °C. The other compounds, such as Oleic acid (OA, 90%), 1-octadecene (ODE, 90%) and polyoxyethylene (5) nonylphenyl ether (Igepal CO-520, Mn = 441), and (3-amino-propyl) triethoxysilane (APS, $\geq 98\%$), were supplied by Beijing InnoChem Science and Technology Co., Ltd. Some common chemical reagents, including NH_4F , NaOH, tetraethylorthosilicate (TEOS), rhodamine B, hydrazine hydrate (85%) and glyoxal, were supplied by Tianjin Chemical Reagents Company. Solvent water was redistilled twice before usage.

2.2. Equipment and Method

Transmission electron microscopy (TEM) and field-emission scanning electron microscopy (FE-SEM) images were provided by a JEM-2010 transmission electron microscope and a Hitachi S-4800 microscope. IR spectra were collected using a Bruker Vertex 70 FT-IR spectrophotometer. XRD curves were collected using a Bruker D4 X-ray diffractometer, Cu K radiation (40 kV, 40 mA). Thermogravimetric analysis (TGA) was finished by a Perkin-Elmer thermal analyzer. Luminescence spectra were recorded by a Hitachi F-4500 spectrophotometer, excited by a CW NIR laser (980 nm).

2.3. The Synthesis for Silica Coated UCNPs

The hydrophobic UCNPs were firstly synthesized following a literature procedure [21]. A typical run was briefly described as follows. A mixture of YCl_3 (0.8 mmol), $YbCl_3$ (0.18 mmol) and $ErCl_3$ (0.02 mmol) in oleic acid (6 mL) and octadecene (15 mL) was loaded into a flask and then heated at 160 °C. After cooling, methanol (10 mL), NaOH (2.5 mmol) and NH_4F (4 mmol) were added into the flask and stirred for half an hour. The resulting mixture was firstly heated at 70 °C for 20 min, then at 100 °C for 10 min and finally at 300 °C for 90 min, within an Ar atmosphere. After natural cooling, cold ethanol was added, white solid was obtained and cleaned with ethanol/water (1:1 v/v). The collected nanocrystals were dispersed in cyclohexane the later use.

A mixture of CO-520 (0.1 mL), cyclohexane (6 mL), hydrophobic UCNPs cyclohexane solution (0.01 M, 4 mL) was stirred for 5 min, then CO-520 (0.4 mL) and ammonia (0.08 mL, 30%) were added. The resulting mixture was treated with ultrasonic bath for 30 min, then TEOS (0.04 mL) was added. The resulting mixture was stirred at room temperature for two days. Acetone was added, and white solid was obtained as silica coated UCNPs which was cleaned with ethanol/water (1:1 v/v) and stored in deionized water.

2.4. Surface Modification on Silica Coated UCNPs

The above obtained silica coated UCNPs (10 mL, 1 mg/mL) was mixed with acetic acid (200 μ L) and APS (10 mL). The resulting mixture was stirred for 180 min under room ambient temperature. Solid product was collected by centrifugation and finally dried in vacuum at 35 °C [22].

2.5. Synthesis of RBO Probe

First, rhodamine hydrazide was synthesized using rhodamine B and hydrazine hydrate as starting chemicals [23]. Then the probe RBO was synthesized by stirring the mixture of rhodamine hydrazide (1 mmol) and glyoxal (2 mL) in ethanol (15 mL) for 18 h under room temperature. Excess NaCl powder was added to yield yellow solid which was further purified on a silica gel column and obtained as RBO. RBO was identified by its 1H NMR data (detailed chemical shift values are listed in Supplementary Materials).

2.6. Synthesis of UCNPs@SiO₂-RBO Nanocomposite

The above obtained silica coated UCNPs (after being modified with APS, 20 mg) was mixed with ethanol (10 mL) and RBO (1 mmol). The resulting mixture was heated at 80 °C for 24 h. Solid product was collected by centrifugation, cleaned with ethanol to eliminate excess RBO, and finally dried in vacuum at 35 °C.

2.7. How to Determine Hg²⁺ with UCNPs@SiO₂-RBO

A suspension of UCNPs@SiO₂-RBO in ethanol/water (7:3, v/v, 0.5 mg/mL, pH = 7) was firstly prepared and then mixed with certain volume of Hg²⁺ standard solution. The resulting mixture was treated with ultrasonic bath for 5 min for a complete mixing, and then sent to record luminescence spectrum. Corresponding excitation and emission wavelengths were set as 980 nm and 540 nm, respectively.

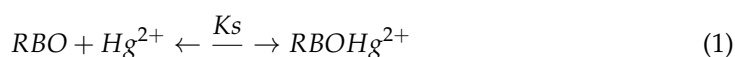
3. Results and Discussion

3.1. Sensing Performance of RBO Probe for Hg²⁺

It is well known that rhodamine-derived molecules all share a structural transformation between a closed-ring structure and an open-ring one. The former structure is non-fluorescent while the latter one is highly fluorescent [21]. Our probe RBO was designed following this protocol, complying with such structural transformation. To ensure the covalent immobilization of RBO probe on the SiO₂ layer of UCNPs, rhodamine hydrazide was reacted with glyoxal and then connected to the amino groups on the SiO₂ layer of UCNPs, so that a nanocomposite UCNPs@SiO₂-RBO was finally obtained. Before discussing the Hg²⁺-sensing performance of UCNPs@SiO₂-RBO, that of probe RBO is firstly explored as follows.

The absorption spectra of RBO upon increasing Hg²⁺ concentration are shown as Figure 1a. The probe RBO obviously responds to Hg²⁺ [21]. The observation of the increasing absorption intensity at 555 nm indicates a structural transformation from a closed-ring structure to an open-ring one, which shall be accompanied with an emission turn on effect. The increasing emission intensity is confirmed by the emission spectra of RBO upon increasing Hg²⁺ concentration, as shown by Figure 1b. Additionally, there is a minor emission red shift (570 nm → 573 nm) with increasing Hg²⁺ concentration. Such emission red shift can be explained by the coordination between RBO and Hg²⁺ which forms a rigid structure and depresses the geometric relaxation in excited state, showing emission red shift.

The chemical stoichiometry of coordination between RBO and Hg²⁺ was further analyzed using Job's titration experiment. Here, the total amount of probe RBO and Hg²⁺ was preserved, with the molar ratio of Hg²⁺ increased from 10% to 90%. Figure 2 shows the emission intensity monitoring at 573 nm. The emission intensity of this RBO-Hg²⁺ mixture firstly increases and then reaches a maximum value at Hg²⁺ molar ratios of 50%. Upon even higher Hg²⁺ molar ratios, the emission intensity decreases gradually. This result suggests a chemical stoichiometry of 1:1 between RBO and Hg²⁺, and corresponding coordination reaction can be described as Equation (1). Here, K_s is the association constant for the coordination reaction between RBO and Hg²⁺.



$$\frac{\alpha}{1 - \alpha} = \frac{1}{K_s [Hg^{2+}]} \quad (2)$$

$$\alpha = \frac{A_T - A_0}{A_T - A_0} \quad (3)$$

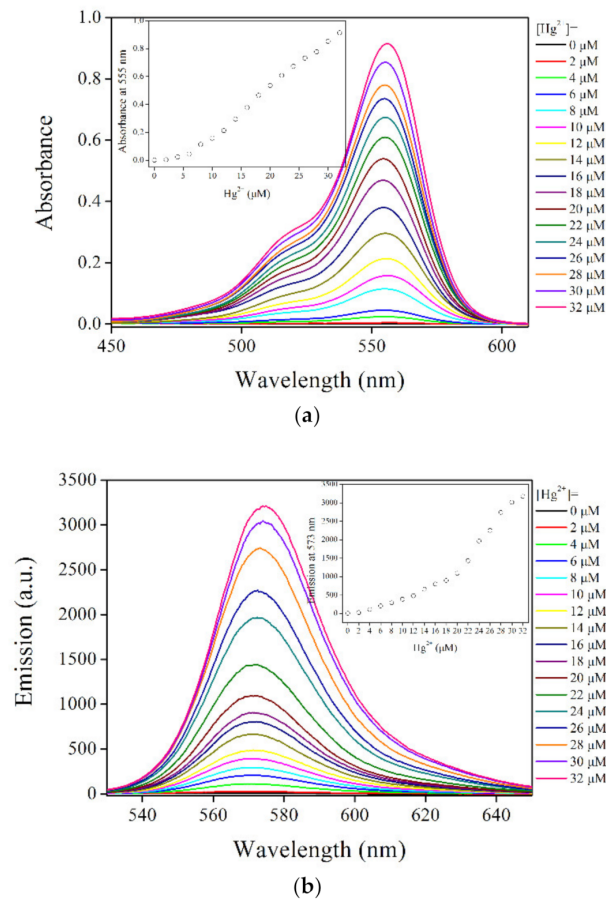


Figure 1. (a) RBO absorption spectra upon various Hg^{2+} concentrations and (b) emission spectra upon various Hg^{2+} concentrations.

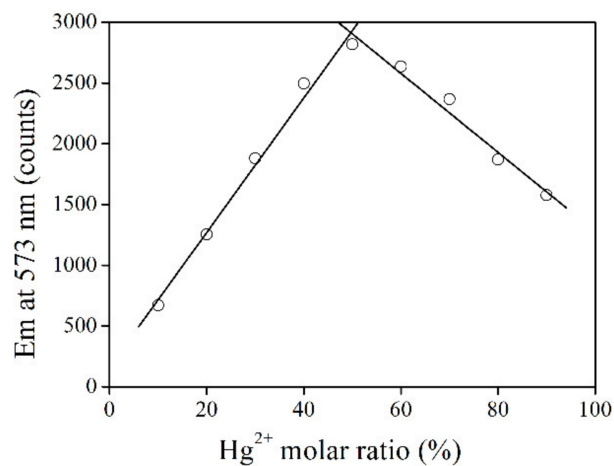


Figure 2. Emission intensity monitoring at 573 nm upon increasing Hg^{2+} molar ratio from 10% to 90%.

K_s of the coordination reaction between RBO and Hg^{2+} is then determined by Equations (2) and (3). Here, A is absorbance value, while A_T and A_0 are the critical absorbance values with $\alpha = 1$ (fully coordinated with Hg^{2+}) and $\alpha = 0$ (no Hg^{2+}), respectively. Based on the absorption spectra in Figure 1, K_s is calculated as $2.6 \times 10^5 \text{ M}^{-1}$ which is found similar to those of rhodamine-derived probes [21]. With the chemical stoichiometry between RBO and Hg^{2+} confirmed, it is assumed that probe RBO shall follow a simple

sensing reaction with Hg^{2+} ions, showing a linear working curve, which consequently benefits sensing operation [21].

Aiming at a fast evaluation on the selectivity of RBO towards Hg^{2+} , its absorption and emission spectra are recorded in the presence of competing metal cations. It is observed from Figure 3 that RBO shows strong absorption peaking at 555 nm only in the presence of Hg^{2+} , suggesting a good selectivity. The competing metal cations are all ineffective in triggering RBO structural transformation, leading to the absence of RBO absorption. Correspondingly, this good selectivity is also observed for the RBO emission case. All competing metal cations are powerless to enhance RBO emission, except for two transition metal cations of Fe^{3+} and Cr^{3+} . Owing to their high ionic charges and thus coordination affinity for RBO, RBO structural transformation is partially initiated by Fe^{3+} and Cr^{3+} , but their unfilled d orbitals play as an emission quencher, which quenches RBO emission dramatically. Nevertheless, a good selectivity of RBO for Hg^{2+} can be confirmed here, making RBO a promising probe for further application.

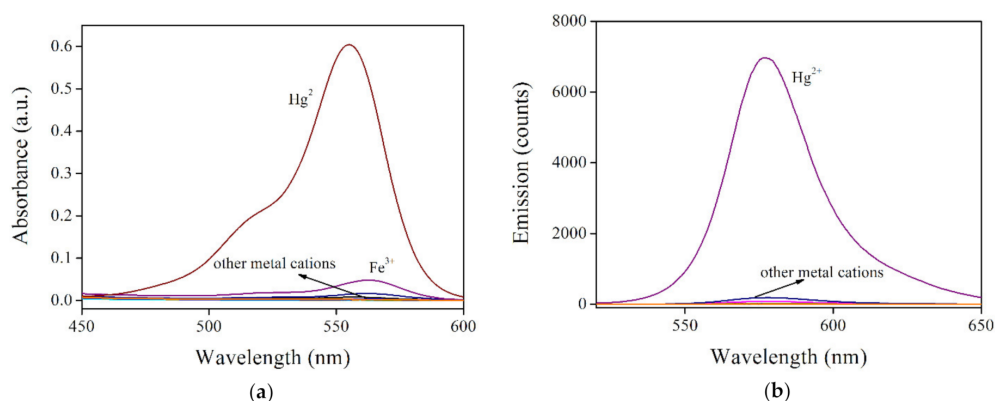
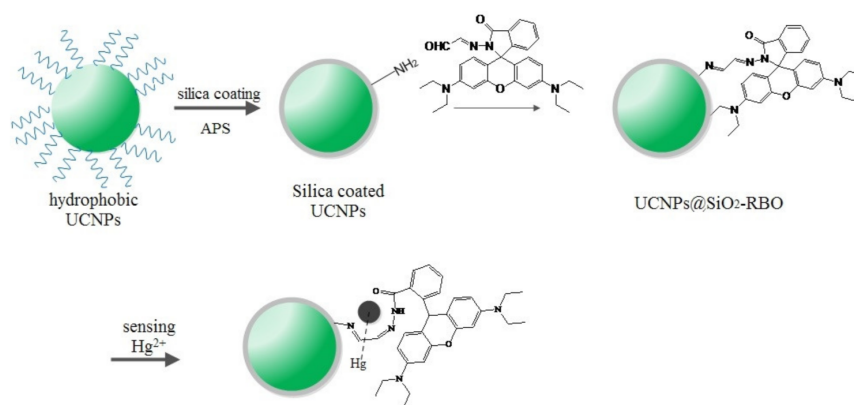


Figure 3. (a). RBO absorption spectra and (b) RBO emission spectra under some metal cations (RBO:cation = 1:1, molar ratio), including K^+ , Ca^{2+} , Mg^{2+} , Pb^{2+} , Co^{2+} , Ni^{2+} , Zn^{2+} , Cd^{2+} , Ag^+ , Cu^{2+} , Fe^{3+} and Hg^{2+} .

3.2. Characterization on UCNP@SiO₂-RBO

After confirming the sensing performance of probe RBO, it can be applied for the construction of nanocomposite. It was found that UCNP with dopants of Yb^{3+} and Er^{3+} have perfect spectral overlapping between their emission bands (~550 nm) and RBO absorption (centering at 555 nm). Scheme 2 illustrates the synthetic route for UCNP@SiO₂-RBO, where the UCNP were used as a secondary excitation source for probe RBO by converting low energy NIR laser (980 nm) to high energy excitation. These UCNP were coated with an amorphous SiO₂ layer so that any potential negative effect from Hg^{2+} and probe RBO are shielded. This SiO₂ layer should not be a thick one so that an efficient energy transfer from UCNP to probe RBO can be finished. UCNP@SiO₂-RBO is carefully characterized below by their SEM images, XRD patterns, IR spectra and TGA data.

Figure 4 shows the SEM image of as-synthesized UCNP so that a visual evaluation on their morphology can be observed. Uniform shape with mean diameter of ~40 nm was observed for these as-synthesized UCNP. Their XRD pattern is shown in Figure 5, which identified their crystalline nature. These labeled XRD peaks are consistent with those of NaYF₄ nanocrystals in hexagonal phase (JCPDS 16-0334), which means that our as-synthesized UCNP were pure hexagonal β -NaYF₄: Yb^{3+} , Er^{3+} nanoparticles. No diffraction peaks from dopants Yb^{3+} and Er^{3+} were observed, indicating that they were successfully doped into β -NaYF₄ crystals without compromising β -NaYF₄ crystalline.



Scheme 2. A synthetic route for probe RBO and its covalent immobilization onto SiO₂-encapsulated UCNPs.

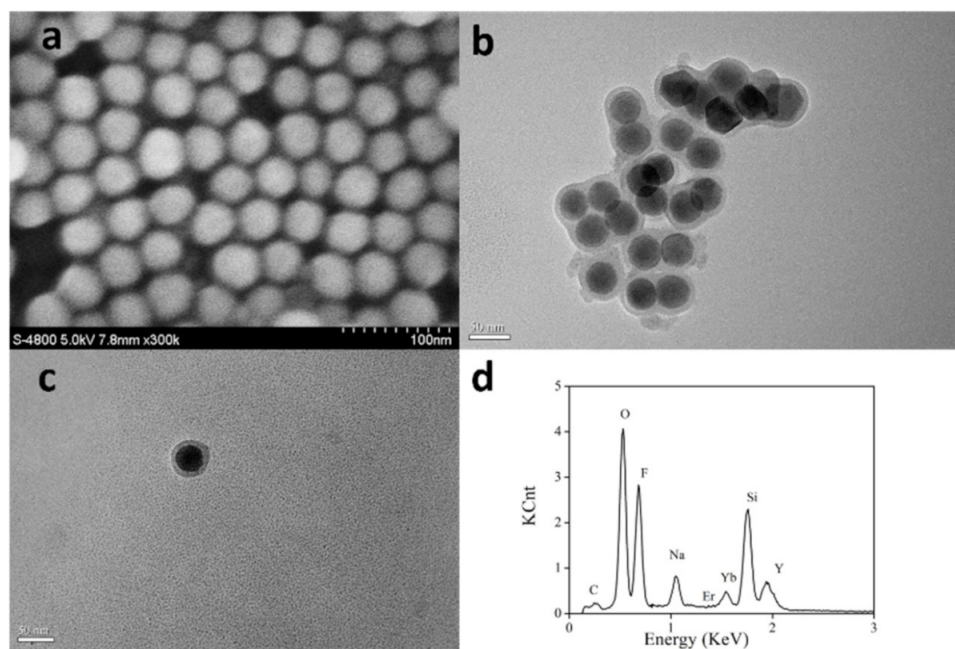


Figure 4. SEM image of as-synthesized UCNPs (a), TEM images of silica coated UCNPs (b) and UCNPs@SiO₂-RBO (c), EDX of silica coated UCNPs (d).

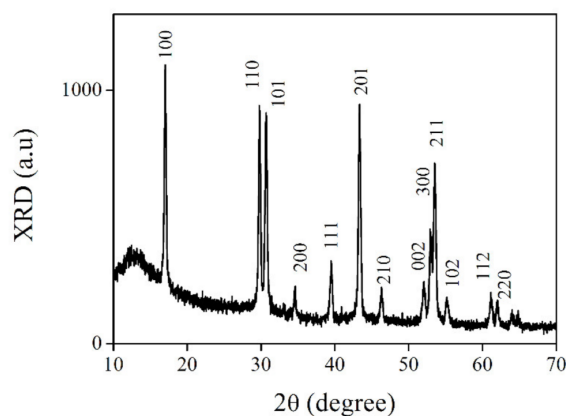


Figure 5. XRD Pattern of As-Synthesized UCNPs.

For all UCNPs synthesized following a classic method in oleic acid, their surface is fully covered by oleic acid chains and thus is highly hydrophobic. To improve the compatibility with Hg^{2+} ions in aqueous media, these UCNPs were coated with amorphous SiO_2 . The resulting silica coated UCNPs were confirmed by their TEM images, as shown in Figure 4. A high resolution TEM suggests that their SiO_2 layer was as thin as 8 nm. The successful SiO_2 coating can be confirmed by the energy dispersive X-ray (EDX) curves of silica coated UCNPs shown in Figure 4.

The covalent probe grafting had increased the diameter of UCNPs@ SiO_2 -RBO to ~45 nm, with a similar morphology to the silica coated UCNPs, as shown in Figure 4. The successful covalent probe grafting between RBO and silica coated UCNPs can be confirmed by comparing the IR spectra of probe RBO, silica coated UCNPs and UCNPs@ SiO_2 -RBO. As shown in Figure 6, a strong IR peak of 1737 cm^{-1} was observed for probe RBO, which can be assigned as the vibration of $-\text{CHO}$ group in RBO. This sharp IR peak is not found from the IR spectrum of UCNPs@ SiO_2 -RBO. A set of IR peaks ranging from 3300 and 3500 cm^{-1} were assigned as the vibration of $-\text{NH}_2$ in amino modified UCNPs. They were not traced in the IR spectrum of UCNPs@ SiO_2 -RBO. However, a new IR band peaking at 1622 cm^{-1} was observed, which was assigned as the vibration of $-\text{N}=\text{CH}-$ group. As a consequence, it is confirmed that probe RBO was successfully immobilized onto the surface of silica coated UCNPs.

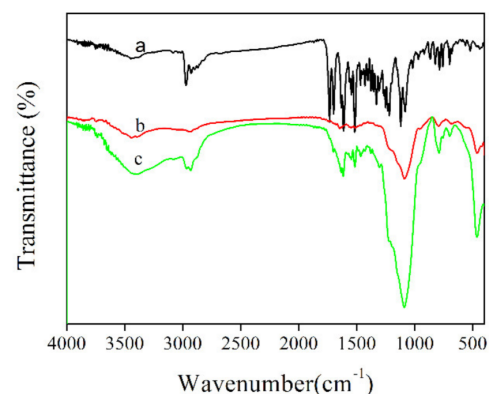


Figure 6. FT-IR spectra of (a) RBO, (b) amino modified UCNPs, (c) UCNPs@ SiO_2 -RBO.

The probe loading amount in UCNPs@ SiO_2 -RBO can be determined by its TGA result. As shown in Figure 7, UCNPs@ SiO_2 -RBO TGA curve is composed of three major weight loss steps, which are localized in temperature regions of $80\text{--}100\text{ }^\circ\text{C}$, $250\text{--}380\text{ }^\circ\text{C}$ and $400\text{--}550\text{ }^\circ\text{C}$, respectively. The first weight loss is slight and thus assigned as the thermal evaporation of physically absorbed water and residual solvent molecules. The second weight loss region is responsible for a weight loss of ~10.5%, with an endothermic peak of $\sim 360\text{ }^\circ\text{C}$. As a consequence, the probe loading amount is determined as 10.5% in UCNPs@ SiO_2 -RBO. Considering this high temperature and obvious weight loss, it is assigned as the thermal destruction of organic probe in UCNPs@ SiO_2 -RBO. The final weight loss region can be assigned as the thermal degradation and collapse of organosilicate frameworks, such as the cleavage of Si-C, C-C and C-N bonds [24,25].

3.3. Energy Transfer in UCNPs@ SiO_2 -RBO

The above result confirms a nanocomposite structure for Hg^{2+} -sensing, which is based on an energy transfer (ET) procedure from UCNPs to Hg^{2+} -sensitive probe RBO. Upon NIR laser of 980 nm , UCNPs excite probe RBO to accomplish the sensing operation.

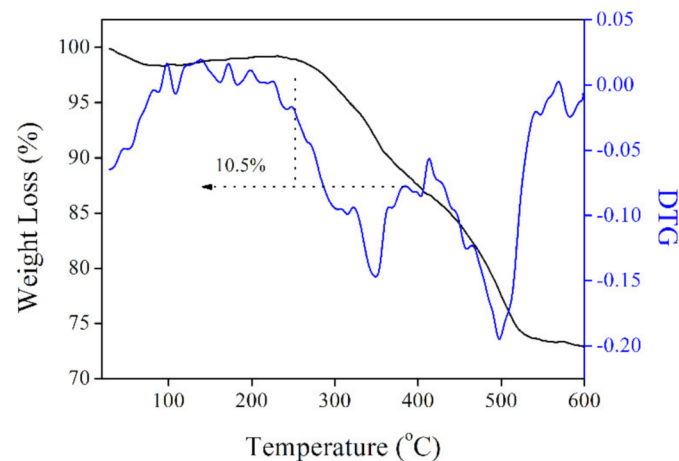


Figure 7. TGA and DTG (differential thermal gravity) curves of UCNPs@SiO₂-RBO.

For the better understanding on the energy transfer between UCNPs and probe RBO, the upconversion emission spectrum of UCNPs and the absorption spectra of RBO, with or without Hg²⁺, are shown in Figure 8. Upon NIR laser excitation of 980 nm, the UCNPs exhibited a major emission band peaking at 540 nm and a shoulder emission band peaking at 521 nm, which can be attributed to ²H_{11/2} to ⁴I_{15/2} transition and ⁴S_{3/2} to ⁴I_{15/2} transition of Er³⁺. There was still a weak band peaking at 650 nm which belonged to the ⁴F_{9/2} to ⁴I_{15/2} transition of Er³⁺. Pure RBO has no obvious absorption within 450 nm to 700 nm. After bonding with Hg²⁺, a strong absorption around 555 nm was observed, which overlaps well with the first two upconversion emission bands of UCNPs, indicating a possibility of energy transfer from UCNPs to RBO. The efficiency of such energy transfer can be evaluated by the Forster radius (R_0) between donor and acceptor, using Equation (4). Here, Q_0 is the intrinsic emission yield of donor in the absence of acceptor, which has been reported as 3% for UCNPs [21]. J is the spectral overlap integral between donor emission and acceptor absorption spectra. κ^2 is mutual molecular orientation factor, N_A is Avogadro number and n_d is solvent refraction index, respectively.

$$R_0^6 = \frac{9Q_0k^2J(\ln 10)}{128\pi^5n_d^4N_A} \quad (4)$$

$$J = \int f_D(\lambda)\varepsilon_A(\lambda)\lambda^4d\lambda$$

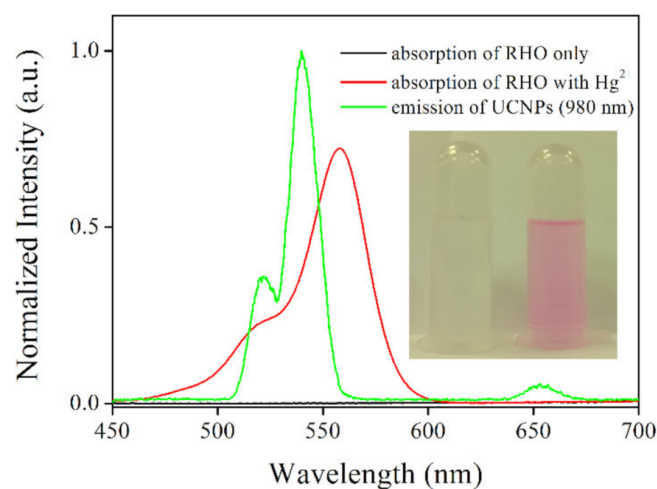


Figure 8. Absorption spectra of RBO and RBO upon addition of Hg²⁺, and emission spectrum of UCNPs (excitation wavelength = 980 nm). Inset: A photo of UCNPs@SiO₂-RBO without Hg²⁺ and with Hg²⁺.

It is observed from Equation (4) that an efficient energy transfer depends on a good spectral overlap between donor emission and acceptor absorption, which has been above confirmed in Figure 8. Additionally, the distance between donor and acceptor has been determined as 8 nm, which is also the thickness of SiO₂ layer. This short distance is positive to improve the energy transfer process. Thus, a fluent energy transfer from UCNP's to RBO can be expected, so that UCNP's green emission can be quenched, showing sensing signal. There is still one issue to be addressed, though. Theoretically, by decreasing the thickness of SiO₂ layer, the distance between donor and acceptor can be decreased, which is supposed to improve the fluorescence resonance energy transfer (FRET) efficiency. On the other hand, a thin layer may lead to the exposure of UCNP's, compromising sensing performance.

3.4. Sensing Performance of UCNP's@SiO₂-RBO

The Hg²⁺-sensing performance of UCNP's@SiO₂-RBO was then analyzed by discussing its emission spectra upon increasing Hg²⁺ concentrations. It is observed from Figure 9 that, upon the NIR laser excitation of 980 nm, the upconversion emission intensity of UCNP's@SiO₂-RBO gradually decreased with Hg²⁺ concentration increased from 0 to 35 μM, showing emission quenching effect. This result actually indicates an energy transfer from UCNP's to probe RBO. For comparison convenience, these emission spectra were analyzed with a modified equation of Stern-Volmer equation, as described as Figure 9 inset. The corresponding regression equation is fitted as $I/I_0 = 5.74 - 0.134[\text{Hg}^{2+}]$ ($R^2 = 0.9992$) with good linearity. The limit of detection (LOD) was determined as 2.2 μM ($3\sigma/N$). This value is found comparable to or even slightly lower than those of similar FRET-based sensing systems for detecting metal cations, as shown in Table 1.

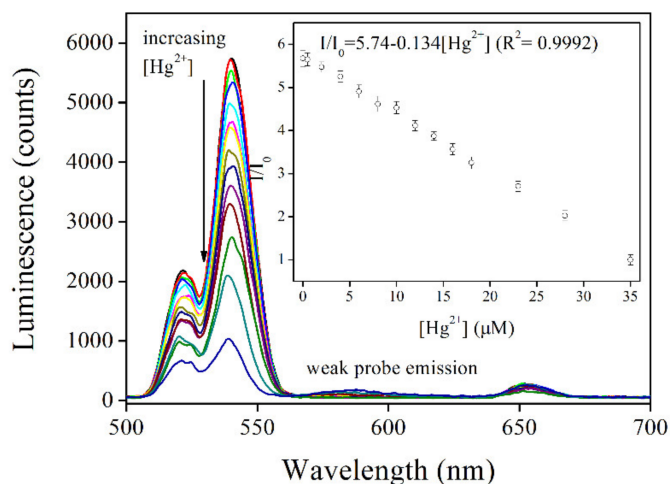


Figure 9. Emission spectra of UCNP's@SiO₂-RBO (0.5 mg/mL) with increasing Hg²⁺ concentration from 0–35 μM in ethanol-water solution (V:V = 7:3). Inset: linear fitting of I/I_0 against Hg²⁺ concentration.

There is an interesting fact worthy of further explanation, though. Even though the probe RBO accepts UCNP's energy and quenches UCNP's emission, there is no obvious RBO emission, which is rather different from the case of free RBO. It has been above confirmed in Figure 1 that RBO shows strong fluorescence in the presence of Hg²⁺. In this case, it is tentatively assumed that the absence of RBO emission in UCNP's@SiO₂-RBO is caused by the self-absorption and self-quenching between probe molecules. It is observed from Figure 1 that the Stokes shift between RBO absorption (555 nm) and emission (573 nm) is rather slim, with efficient spectral overlap between RBO absorption and emission spectra. Due to the restriction of secondary excitation mechanism and the low quantum yield of UCNP's (3%), RBO emission is weak. This weak emission may be absorbed by surrounding RHO molecules in ground state. As a consequence, no obvious RBO emission shows.

Table 1. Key sensing parameters of UCNPs@SiO₂-RBO and literature systems. LOD = limit of detection.

Name	Sensitivity	Sensing Type	Linearity	LOD	Ref.
UCNPs@SiO ₂ -RHO	5.67	quenching	linear	2.2 μM	this work
UCNPs&RB-hydrazide	~2.9	ratiometric	linear	10 ⁻⁶ M	[26]
Si-RH	~2.2	emission turn on	linear	2.7 nM	[23]
CS1	~0.4	absorption turn on	linear	N/A	[27]
RbCS	N/A	emission turn on	non-linear	N/A	[28]

Finally, the sensing selectivity of UCNPs@SiO₂-RBO for Hg²⁺ is discussed as follows. Some common interfering metal cations were selected here, including K⁺, Ca²⁺, Mg²⁺, Pb²⁺, Co²⁺, Ni²⁺, Zn²⁺, Cd²⁺, Ag⁺, Cu²⁺ and Fe³⁺. Their nitrate salts were added into the solution of UCNPs@SiO₂-RBO; corresponding emission intensity variation is shown in Figure 10. It was observed that these interfering metal cations exert no obvious effect on the luminescence intensity of UCNPs@SiO₂-RBO. Only the presence of Hg²⁺ leads to an obvious emission quenching. Even in a mixture of these interfering metal ions, such luminescence quenching was still observed. This good selectivity can certainly be attributed to probe RBO's unique sensing mechanism towards Hg²⁺, and after being immobilized onto the surface of UCNPs, such good selectivity is still preserved. Hereby, it is finally concluded that UCNPs@SiO₂-RBO is a selective Hg²⁺-sensing nanocomposite excited by NIR laser of 980 nm.

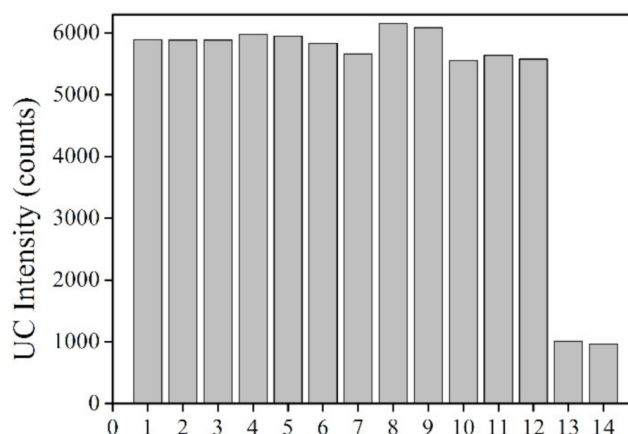


Figure 10. Interfering metal cations effect (100 μM) on emission intensity of UCNPs@SiO₂-RBO (0.5 mg/mL) in ethanol-water solution (V:V = 7:3). 1 = no ion, 2 = K⁺, 3 = Ca²⁺, 4 = Pb²⁺, 5 = Mg²⁺, 6 = Co²⁺, 7 = Ni²⁺, 8 = Zn²⁺, 9 = Cd²⁺, 10 = Ag⁺, 11 = Cu²⁺, 12 = Fe²⁺, 13 = Hg²⁺ (only), 14 = Hg²⁺ (mixed with all the above metal ions).

4. Conclusions

In this paper, we reported a rhodamine-derived probe RBO for Hg²⁺ sensing. It was found that both RBO absorption and emission intensity were increased with increasing Hg²⁺, showing obvious sensing signal. The chemical stoichiometry analysis suggested a simple coordination reaction between RBO and Hg²⁺ with molar ratio of 1:1. The association constant was determined as $2.6 \times 10^5 \text{ M}^{-1}$. This high affinity confirmed a coordination reaction between RBO and Hg²⁺. Probe RBO showed good selectivity for Hg²⁺, even in the presence of interfering metal cations. By covalently grafting RBO onto UCNPs, a nanocomposite sensing system was constructed, which absorbed NIR laser excitation of 980 nm and transferred this energy to probe RBO, showing the emission quenching effect of UCNPs. A linear working curve was observed, with LOD value of 2.2 μM. There was an interesting fact that had never been reported by other references,

which was the emission absence of probe RBO, even though it accepted UCNPs energy. The self-absorption and self-quenching between probe molecules was claimed responsible for this phenomenon. This UCNPs-based nanocomposite applied NIR as excitation source. As a consequence, low background noise of autofluorescence was observed. This method can be used as a promising pathway for the detection in biological samples.

Supplementary Materials: The following are available online at <https://www.mdpi.com/2073-4352/11/2/104/s1>.

Author Contributions: W.W. (Wei Wu) was responsible for original draft, review and final editing. W.W. (Wei Wei) was responsible for methodology. D.X. was responsible for experiment investigation. Y.L. was responsible for formal analysis of experiment result. J.L. was responsible for supervision and software application. K.G. was responsible for supervision. L.L. was responsible for draft preparation, writing, review and editing. All authors have read and agreed to the published version of the manuscript.

Funding: This research was funded by the Natural Science Foundation of Zhejiang, China (Grant No. LQ21H060002), Zhejiang Provincial Natural Science Foundation of China under Grant No.LQ20H060002, the Natural Science Foundation of Ningbo, China (Grant No. 2019A610247 and Grant No. 202003N4324), “Scientific and Technological innovation 2025” Major Project (Grant No.2019B10062), Research Foundation of Hwa Mei Hospital, University of Chinese Academy of Sciences, China (Grant No.2020HMKY16) and Project of the Science and Technology Plan for Zhejiang Province(LGF21F020022) and The APC was funded by Zhejiang Provincial Natural Science Foundation of China under Grant No.LQ20H060002 and “Scientific and Technological innovation 2025” Major Project (Grant No.2019B10062).

Acknowledgments: The authors gratefully thank below financial supports, including the Natural Science Foundation of Zhejiang, China (Grant No. LQ21H060002), Zhejiang Provincial Natural Science Foundation of China under Grant No.LQ20H060002, the Natural Science Foundation of Ningbo, China (Grant No. 2019A610247 and Grant No. 202003N4324), “Scientific and Technological innovation 2025” Major Project (Grant No.2019B10062), Research Foundation of Hwa Mei Hospital, University of Chinese Academy of Sciences, China (Grant No.2020HMKY16) and Project of the Science and Technology Plan for Zhejiang Province(LGF21F020022).

Conflicts of Interest: The authors declare no conflict of interest.

References

1. Wang, Q.; Kim, D.; Dionysiou, D.D.; Sorial, G.A.; Timberlake, D. Sources and remediation for mercury contamination in aquatic systems—a literature review. *Environ. Pollut.* **2004**, *131*, 323. [[CrossRef](#)] [[PubMed](#)]
2. Nolan, E.M.; Lippard, S.J. A “Turn-On” fluorescent sensor for the selective detection of mercuric ion in aqueous media. *J. Am. Chem. Soc.* **2003**, *125*, 14270. [[CrossRef](#)] [[PubMed](#)]
3. Yoon, S.; Miller, E.W.; He, Q.; Do, P.H.; Chang, C.J. A bright and specific fluorescent sensor for mercury in water, cells, and tissue. *Angew. Chem. Int. Ed.* **2007**, *46*, 6658. [[CrossRef](#)] [[PubMed](#)]
4. Wanichancheva, N.; Setthakarn, K.; Prapawattanapol, N.; Hanmeng, O.; Lee, V.S.; Grudpan, K. Rhodamine B-based “turn-on” fluorescent and colorimetric chemosensors for highly sensitive and selective detection of mercury (II) ions. *J. Lumin.* **2012**, *132*, 35. [[CrossRef](#)]
5. Park, M.; Seo, S.; Lee, I.S.; Jung, J.H. Ultraefficient separation and sensing of mercury and methylmercury ions in drinking water by using aminonaphthalimide-functionalized Fe₃O₄@SiO₂ core/shell magnetic nanoparticles. *Chem. Commun.* **2010**, *46*, 4478. [[CrossRef](#)]
6. Duan, J.; Jiang, X.; Ni, S.; Yang, M.; Zhan, J. Facile synthesis of N-acetyl-L-cysteine capped ZnS quantum dots as an eco-friendly fluorescence sensor for Hg²⁺. *Talanta* **2011**, *85*, 1738. [[CrossRef](#)]
7. Li, H.; Wang, L. NaYF₄:Yb³⁺/Er³⁺ nanoparticle-based upconversion luminescence resonance energy transfer sensor for mercury(II) quantification. *Analyst* **2013**, *138*, 1589. [[CrossRef](#)]
8. Li, C.; Liu, J.; Alonso, S.; Li, F.; Zhang, Y. Upconversion nanoparticles for sensitive and in-depth detection of Cu²⁺ ions. *Nanoscale* **2012**, *4*, 6065. [[CrossRef](#)]
9. Li, C.; Lin, J. Rare earth fluoride nano-/microcrystals: Synthesis, surface modification and application. *J. Mater. Chem.* **2010**, *20*, 6831. [[CrossRef](#)]
10. Haase, M.; Schafer, H. Upconverting nanoparticles. *Angew. Chem. Int. Ed.* **2011**, *50*, 5808. [[CrossRef](#)]
11. Chatterjee, D.K.; Rufaihah, A.J.; Zhang, Y. Upconversion fluorescence imaging of cells and small animals using lanthanide doped nanocrystals. *Biomaterials* **2008**, *29*, 937. [[CrossRef](#)] [[PubMed](#)]

12. Bouzigues, C.; Gacoin, T.; Alexandrou, A. Biological applications of rare-earth based nanoparticles. *ACS Nano*. **2011**, *5*, 8488. [[CrossRef](#)] [[PubMed](#)]
13. Shan, G.; Weissleder, R.; Hilderbrand, S.A. Upconverting organic dye doped core-shell nano-composites for dual-modality nir imaging and photo-thermal therapy. *Theranostics* **2013**, *3*, 267. [[CrossRef](#)] [[PubMed](#)]
14. Pierre, A.T.V.C. Principles of responsive lanthanide-based luminescent probes for cellular imaging. *Anal. Bioanal. Chem.* **2009**, *394*, 107.
15. Boyer, J.C.; Manseau, M.P.; Murray, J.I.; Van Veggel, F.C.J.M. Surface modification of upconverting NaYF₄ nanoparticles with peg–phosphate ligands for nir (800 nm) biolabeling within the biological window. *Langmuir* **2010**, *26*, 1157. [[CrossRef](#)]
16. Liu, J.; Cheng, J.; Zhang, Y. Upconversion nanoparticle based LRET system for sensitive detection of MRSA DNA sequence. *Biosens. Bioelectron.* **2013**, *43*, 252. [[CrossRef](#)]
17. Wang, L.; Yan, R.; Huo, Z.; Wang, L.; Zeng, J.; Bao, J.; Wang, X.; Peng, Q.; Li, Y. Fluorescence resonant energy transfer biosensor based on upconversion-luminescent nanoparticles. *Angew. Chem. Int. Ed.* **2005**, *44*, 6054. [[CrossRef](#)]
18. Yao, L.; Zhou, J.; Liu, J.; Feng, W.; Li, F. Iridium-complex-modified upconversion nanophosphors for effective lret detection of cyanide anions in pure water. *Adv. Funct. Mater.* **2012**, *22*, 2667. [[CrossRef](#)]
19. Siefe, C.; Mehlenbacher, R.D.; Peng, C.S.; Zhang, Y.; Fischer, S.; Lay, A.; McLellan, C.A.; Alivisatos, A.P.; Chu, S.; Dionne, J.A. Sub-20 nm core–shell–shell nanoparticles for bright upconversion and enhanced förster resonant energy transfer. *J. Am. Chem. Soc.* **2019**, *141*, 16997–17005. [[CrossRef](#)]
20. Kang, D.; Lee, S.; Shin, H.; Pyun, J.; Lee, J. An efficient NIR-to-NIR signal-based LRET system for homogeneous competitive immunoassay. *Biosens. Bioelectron.* **2020**, *150*, 111921. [[CrossRef](#)]
21. Li, Z.; Liang, T.; Wang, Q.; Liu, Z. Strategies for constructing upconversion luminescence nanoprobe to improve signal contrast. *Small* **2020**, *16*, 1905084. [[CrossRef](#)] [[PubMed](#)]
22. Yuan, P.; Lee, Y.H.; Gnanasammandhan, M.K.; Guan, Z.; Zhang, Y.; Xu, Q.H. Plasmon enhanced upconversion luminescence of NaYF₄:Yb,Er@SiO₂@Ag core–shell nanocomposites for cell imaging. *Nanoscale* **2012**, *4*, 5132. [[CrossRef](#)] [[PubMed](#)]
23. Ni, J.; Li, Q.; Li, B.; Zhang, L. A novel fluorescent probe based on rhodamine B derivative for highly selective and sensitive detection of mercury(II) ion in aqueous solution. *Sens. Actuators B* **2013**, *186*, 278. [[CrossRef](#)]
24. Li, Y.J.; Yan, B. Lanthanide (Eu³⁺, Tb³⁺)/β-diketone modified mesoporous sba-15/organic polymer hybrids: Chemically bonded construction, physical characterization, and photophysical properties. *Inorg. Chem.* **2009**, *48*, 8276. [[CrossRef](#)] [[PubMed](#)]
25. Wang, L.; Li, B.; Zhang, L.; Zhang, L.; Zhao, H. Fabrication and characterization of a fluorescent sensor based on Rh 6G-functionlized silica nanoparticles for nitrite ion detection. *Sens. Actuators B* **2012**, *171–172*, 946. [[CrossRef](#)]
26. Zhang, J.; Li, B.; Zhang, L.; Jiang, H. An optical sensor for Cu(II) detection with upconverting luminescent nanoparticles as an excitation source. *Chem. Commun.* **2012**, *48*, 4860. [[CrossRef](#)]
27. Xie, X.; Chen, X.; Li, B.; Zhang, L. Study on a highly selective colorimetric chemosensor for Cu²⁺ detection and its indirect sensing for hypochlorite. *Dye. Pigment.* **2013**, *98*, 433. [[CrossRef](#)]
28. Yang, Y.; Gao, C.; Li, B.; Xu, L.; Duan, L. A rhodamine-based colorimetric and reversible fluorescent chemosensor for selectively detection of Cu²⁺ and Hg²⁺ ions. *Sens. Actuators B* **2014**, *199*, 121. [[CrossRef](#)]